

Derivation of a non-local interfacial Hamiltonian for short-ranged wetting: II. General diagrammatic structure

This article has been downloaded from IOPscience. Please scroll down to see the full text article.

2007 J. Phys.: Condens. Matter 19 416105

(<http://iopscience.iop.org/0953-8984/19/41/416105>)

View [the table of contents for this issue](#), or go to the [journal homepage](#) for more

Download details:

IP Address: 129.252.86.83

The article was downloaded on 29/05/2010 at 06:13

Please note that [terms and conditions apply](#).

Derivation of a non-local interfacial Hamiltonian for short-ranged wetting: II. General diagrammatic structure

A O Parry¹, C Rascón², N R Bernardino¹ and J M Romero-Enrique³

¹ Department of Mathematics, Imperial College London, London SW7 2BZ, UK

² Grupo Interdisciplinar de Sistemas Complejos (GISC), Departamento de Matemáticas, Universidad Carlos III de Madrid, 28911 Leganés (Madrid), Spain

³ Departamento de Física Atómica, Molecular y Nuclear, Universidad de Sevilla, Apartado de Correos 1065, 41080 Seville, Spain

Received 4 July 2007, in final form 5 July 2007

Published 10 September 2007

Online at stacks.iop.org/JPhysCM/19/416105

Abstract

In our first paper, we showed how a non-local effective Hamiltonian for short-ranged wetting may be derived from an underlying Landau–Ginzburg–Wilson model. Here, we combine the Green’s function method with standard perturbation theory to determine the general diagrammatic form of the binding potential functional beyond the double-parabola approximation for the Landau–Ginzburg–Wilson bulk potential. The main influence of cubic and quartic interactions is simply to alter the coefficients of the double parabola-like zigzag diagrams and also to introduce curvature and tube-interaction corrections (also represented diagrammatically), which are of minor importance. Non-locality generates effective long-ranged many-body interfacial interactions due to the reflection of tube-like fluctuations from the wall. Alternative wall boundary conditions (with a surface field and enhancement) and the diagrammatic description of tricritical wetting are also discussed.

1. Introduction

In [1], we showed how a non-local interfacial Hamiltonian for short-ranged wetting [2] may be derived from a Landau–Ginzburg–Wilson model using a diagrammatic formalism based on Green’s functions [3]. While the definition of the interfacial model is the same as that forwarded by other authors [4–6], its evaluation is non-perturbative in the interfacial gradient and reveals important non-local features. This has a number of advantages [7, 8] over previous, local approximations, and appears to overcome a series of problems associated with short-ranged wetting [4–15]. The interaction of the interface and wall is described by a binding potential functional W which has an elegant diagrammatic expansion

$$W = a_1 \text{L} + b_1 \text{V} + \dots \quad (1)$$

and an appealing physical interpretation as tube-like fluctuations [16] which zigzag between the surfaces.

In this paper, we demonstrate the robustness of the diagrammatic expansion by extending the derivation beyond the double-parabola (DP) approximation for the bulk thermodynamic potential appearing in the Landau–Ginzburg–Wilson (LGW) Hamiltonian. We establish the general form of the asymptotic expansion of W , which now includes diagrams representing curvature corrections and tube–tube interactions. However, these are of negligible importance and the above diagrammatic expression remains valid, albeit with numerical changes to the values of the coefficients a_1 and b_1 , which can be determined exactly.

Our article is arranged as follows: after recapping briefly the central results of [1], sections 3–6 describe the detailed derivation of W beyond DP using the same diagrammatic formalism. The proof is rather technical and, to simplify things, we continue using fixed boundary conditions at the wall until the final section. Sections 7–9 are a lengthy discussion of the interpretation of the model and the evaluation of the diagrams for wetting transitions at planar walls which extends the analysis given in [1]. In particular, non-locality is shown to induce weak but long-ranged two-body interactions describing the repulsion of the interface from the wall. Alternative forms of boundary conditions, including coupling to an external surface field and enhancement [17] and diagrams describing tricritical wetting, are also discussed.

2. Wetting diagrams within the double-parabola approximation

We begin with some general considerations. Imagine a system bounded by a wall described by a height function $\psi(\mathbf{x})$ measured above some reference plane with parallel vector displacement $\mathbf{x} = (x, y)$ (see figure 1). The wall is in contact with a fluid phase α but preferentially adsorbs a fluid phase β which forms a thin film intervening between the bulk α phase and the wall. Throughout our paper, we will restrict our attention to the case of bulk two-phase coexistence, although it is easy to extend the analysis to non-zero values of the bulk ordering field. For systems with short-ranged forces, a convenient microscopic starting point for studying this is the continuum LGW Hamiltonian

$$H[m] = \int d\mathbf{r} \left\{ \frac{1}{2}(\nabla m)^2 + \Delta\phi(m) \right\} \quad (2)$$

based on a magnetization-like order parameter $m(\mathbf{r})$. A bulk potential $\phi(m)$ describes the coexistence of the phases α and β , which, on imposing Ising symmetry, we identify with the spontaneous magnetizations $-m_0$ and $+m_0$ respectively. The relative potential $\Delta\phi(m) = \phi(m) - \phi(m_0)$ is introduced to remove from the total free energy a contribution proportional to the volume.

From (2), we wish to derive the form of an interfacial Hamiltonian pertinent to an ‘ m^4 ’ bulk potential

$$\phi(m) = -\frac{r}{2} m^2 + \frac{u}{4} m^4 \quad (3)$$

below the bulk critical temperature (see figure 2). Bulk-like fluctuations are treated in mean-field fashion, so the latter condition implies $r > 0$. Written in terms of the mean-field spontaneous magnetization $m_0 = \sqrt{r/u}$, and inverse bulk correlation length $\kappa = \sqrt{2r}$, the relative potential is

$$\Delta\phi(m) = \frac{\kappa^2}{8m_0^2} (m^2 - m_0^2)^2. \quad (4)$$

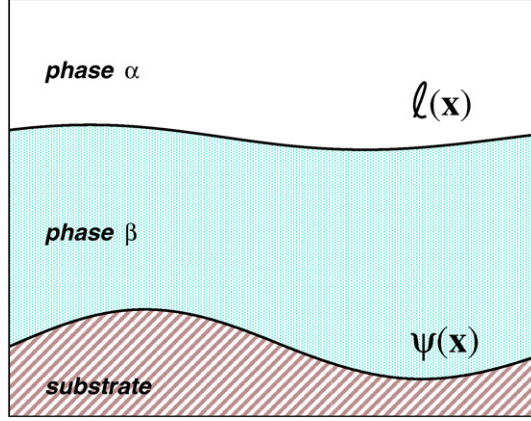


Figure 1. Schematic diagram showing a wetting layer of phase β at a non-planar wall- α interface. Here, $\ell(\mathbf{x})$ and $\psi(\mathbf{x})$ are the interfacial collective coordinate and wall height, respectively. (This figure is in colour only in the electronic version)

For later purposes, it is convenient to re-express this as

$$\Delta\phi(m) = \frac{\kappa^2}{2} \delta m^2 \left\{ 1 + \frac{\delta m}{m_0} + \frac{1}{4} \frac{\delta m^2}{m_0^2} \right\} \quad (5)$$

where we have defined $\delta m = |m| - m_0$. A much easier starting point for analysis is the DP approximation [18]

$$\Delta\phi^{(0)}(m) = \frac{\kappa^2}{2} (|m| - m_0)^2 \quad (6)$$

in which one neglects the higher-order cubic and quartic terms [4] (see figure 2). The superscript indicates that the LGW model with a DP potential is the starting point for our perturbation theory. We define the reference Hamiltonian

$$H^{(0)}[m] = \int d\mathbf{r} \left\{ \frac{1}{2} (\nabla m)^2 + \Delta\phi^{(0)}(m) \right\}. \quad (7)$$

Finally, we adopt the simplest choice of boundary condition corresponding to fixed surface magnetization. Thus, if $\mathbf{r}_\psi = (\mathbf{x}, \psi(\mathbf{x}))$ denotes an arbitrary point on the wall, we require

$$m(\mathbf{r}_\psi) = m_1, \quad (8)$$

for a fixed value of m_1 . Without loss of generality, we set $m_1 > 0$ so that the wall preferentially adsorbs a thin layer of net positive (β -like) magnetization. For both the DP and the full ‘ m^4 ’ models, the mean-field wetting phase boundary, as defined for a planar wall, corresponds to $m_1 = m_0$. That is, for $m_1 < m_0$ the planar wall- β interface is partially wetted (with finite contact angle θ) and the $\alpha|\beta$ interface unbinds continuously as $m_1 \rightarrow m_0^-$. The wall is completely wetted by the β phase for $m_1 > m_0$, corresponding to $\theta = 0$. Note that, with these boundary conditions, first-order and tricritical wetting transitions do not arise. It is convenient to introduce a dimensionless temperature-like scaling field

$$t = \frac{m_1 - m_0}{m_0} \quad (9)$$

which measures the deviation from the three-dimensional critical wetting phase boundary.

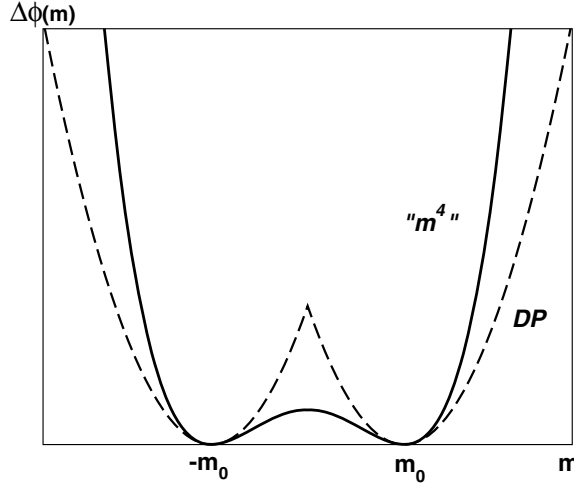


Figure 2. The relative potential $\Delta\phi(m)$ in the ‘ m^4 ’ theory (4) and DP approximation (6) at bulk coexistence.

Following Fisher and Jin [4, 5] we define the interfacial co-ordinate $\ell(\mathbf{x})$ using a crossing criterion and consider constrained profiles which have a surface of iso-magnetization $m^X = 0$ at some prescribed interfacial configuration:

$$m(\mathbf{r}_\ell) = 0 \quad (10)$$

for all points $\mathbf{r}_\ell = (\mathbf{x}, \ell(\mathbf{x}))$. Starting from a suitable microscopic model $H[m]$, the interfacial Hamiltonian $H[\ell, \psi]$ is defined via a partial trace over this class of constrained profiles. A saddle point approximation leads to the Fisher–Jin identification

$$H[\ell, \psi] = H[m_\Xi(\mathbf{r})] - F_{w\beta}[\psi] \quad (11)$$

where $F_{w\beta}[\psi]$ is the excess free energy of the wall– β interface. Here $m_\Xi(\mathbf{r})$ is the constrained profile that minimizes the LGW Hamiltonian with the appropriate boundary conditions at the interface and wall and in the bulk. That is, the constrained profile satisfies the variational equation

$$\left. \frac{\delta H[m]}{\delta m} \right|_{m_\Xi(\mathbf{r})} = 0. \quad (12)$$

We now focus on the properties of the DP model (7), summarizing the main results of our previous article. The variational equation (12) leads to the Helmholtz equation

$$\nabla^2 \delta m_\Xi^{(0)} = \kappa^2 \delta m_\Xi^{(0)} \quad (13)$$

where $\delta m_\Xi \equiv |m_\Xi| - m_0$. Again, the superscript (not used in [1]) serves to indicate that the DP potential is the zeroth-order term in a perturbative expansion. The linearity of these equations simplifies considerably the derivation of the non-local model. Making use of the divergence theorem,

$$H^{(0)}[m_\Xi^{(0)}] = -\frac{\delta m_1}{2} \int_\psi d\mathbf{s}_\psi \nabla m_\Xi^{(0)} \cdot \mathbf{n}_\psi - \frac{m_0}{2} \int_{\ell^-} d\mathbf{s}_\ell \nabla m_\Xi^{(0)} \cdot \mathbf{n}_\ell - \frac{m_0}{2} \int_{\ell^+} d\mathbf{s}_\ell \nabla m_\Xi^{(0)} \cdot \mathbf{n}_\ell \quad (14)$$

contains only surface terms. Here, $\delta m_1 = m_1 - m_0$ while \mathbf{n}_ψ and \mathbf{n}_ℓ denote the (local) unit normals at the wall and interface respectively, pointing into the bulk. Similarly, the infinitesimals ds_ψ and ds_ℓ represent local area elements at the wall and interface. The solutions to the Helmholtz equations in the bulk ($m_\Xi < 0$) and wetting ($m_\Xi > 0$) regions are written in terms of the Green's function

$$K(\mathbf{r}_1, \mathbf{r}_2) = \frac{\kappa}{2\pi|\mathbf{r}_1 - \mathbf{r}_2|} e^{-\kappa|\mathbf{r}_1 - \mathbf{r}_2|} \quad (15)$$

which satisfies the Ornstein–Zernike-like equation

$$(-\nabla_{\mathbf{r}_1}^2 + \kappa^2) K(\mathbf{r}_1, \mathbf{r}_2) = 2\kappa\delta(\mathbf{r}_1 - \mathbf{r}_2) \quad (16)$$

and decays to zero as $|\mathbf{r}_1 - \mathbf{r}_2| \rightarrow \infty$. We represent this Green's function diagrammatically by a straight thick line with the open circles denoting the end points

$$K(\mathbf{r}_1, \mathbf{r}_2) = \int . \quad (17)$$

Using the Green's function, we identify the constrained magnetization $m_\Xi^{(0)}$ in the bulk region

$$m_\Xi^{(0)} = -m_0 + m_0 \text{---} \text{---} \quad (18)$$

and, within the wetting layer, via the expansion

$$\delta m_\Xi^{(0)} = -m_0 \left(\text{---} \text{---} - \text{---} \text{---} + \text{---} \text{---} - \dots \right) + \delta m_1 \left(\text{---} \text{---} - \text{---} \text{---} + \text{---} \text{---} - \dots \right). \quad (19)$$

In this diagrammatic notation, the wavy lines represent the constrained interfacial configuration (top) and wall (bottom), while a black dot on a surface means one must integrate over all points on that surface with the appropriate infinitesimal area element. These expressions are exact solutions to the Helmholtz equations, and satisfy the boundary conditions at the interface and wall to exponentially accurate order in the radii of curvature.

After substituting into (14) and making use of the method of images, we arrive at the desired result

$$H^{(0)}[\ell, \psi] = H_{\alpha\beta}^{(0)}[\ell] + W^{(0)}[\ell, \psi] \quad (20)$$

where

$$H_{\alpha\beta}^{(0)}[\ell] = \Sigma_{\alpha\beta}^{(0)} A_{\alpha\beta} \quad (21)$$

is the interfacial Hamiltonian of the free $\alpha|\beta$ interface, $A_{\alpha\beta}$ is the interfacial area and $\Sigma_{\alpha\beta}^{(0)} = \kappa m_0^2$ is the DP result for the interfacial tension. The binding potential functional is given by

$$W^{(0)}[\ell, \psi] = \sum_{n=1}^{\infty} \left\{ a_1^{(0)} \Omega_n^n + b_1^{(0)} \Omega_n^{n+1} + b_2^{(0)} \Omega_{n+1}^n \right\} \quad (22)$$

with geometry independent coefficients

$$\frac{a_1^{(0)}}{\kappa m_0^2} = 2t, \quad \frac{b_1^{(0)}}{\kappa m_0^2} = 1, \quad \frac{b_2^{(0)}}{\kappa m_0^2} = t^2 \quad (23)$$

and Ω_μ^v correspond to surface integrals over products of the kernel K . The diagrammatic and algebraic representations of the first three terms are

$$\Omega_1^1[\ell, \psi] = \text{---} \text{---} = \int \int ds_\psi ds_\ell K(\mathbf{r}_\psi, \mathbf{r}_\ell) \quad (24)$$

$$\Omega_1^2[\ell, \psi] = \text{---} \text{---} = \int ds_\psi \left\{ \int ds_\ell K(\mathbf{r}_\psi, \mathbf{r}_\ell) \right\}^2 \quad (25)$$

$$\Omega_2^1[\ell, \psi] = \text{---} \text{---} = \int ds_\ell \left\{ \int ds_\psi K(\mathbf{r}_\psi, \mathbf{r}_\ell) \right\}^2 \quad (26)$$

although for certain configurations further simplification is possible (see later). All diagrams have a zigzag structure, for example,

$$\Omega_2^2[\ell, \psi] = \text{Diagram 1}, \quad \Omega_2^3[\ell, \psi] = \text{Diagram 2}.$$

Thus, up to ‘two tubes’, the asymptotic expansion of W is

$$W^{(0)} = a_1^{(0)} \text{Diagram 1} + b_1^{(0)} \text{Diagram 2} + b_2^{(0)} \text{Diagram 3} + \dots \quad (27)$$

with the higher-order terms resumming to give the hard-wall repulsion of the wall.

The coefficient of each diagram Ω_μ^ψ has the dimensions of a surface tension and exhibits a power-law dependence on the scaling field t . A handy rule to remember is that the power of t is the same as the number of black dots on the wall that are singly connected, i.e. have only one kernel K attached to them. This rule also applies to all diagrams containing only black dots which will be generated in the perturbation series described next.

One also generates an expression for the excess free energy of the wall- β interface

$$F_{w\beta}^{(0)}[\psi] = \Sigma_{w\beta}^{(0)} A_w + C_{w\beta}^{(0)} \int ds_\psi \left\{ \frac{1}{R_1^\psi} + \frac{1}{R_2^\psi} \right\} \quad (28)$$

which depends on the area A_w and the mean curvature of the wall. The latter are expressed in terms of the local principal radii of curvature R_1^ψ and R_2^ψ . The tension and rigidity are given by $\Sigma_{w\beta}^{(0)} = \kappa m_0^2 t^2/2$ and $C_{w\beta}^{(0)} = m_0^2 t^2/4$ respectively.

Finally, for wetting at planar substrates ($\psi = 0$) the non-local model recovers the known form of the approximate local interfacial Hamiltonian when $\nabla\ell \ll 1$. We find

$$H^{(0)}[\ell] \approx \int d\mathbf{x} \left\{ \frac{\Sigma^{(0)}(\ell)}{2} (\nabla\ell)^2 + W_\pi^{(0)}(\ell) \right\} + \Sigma_{\alpha\beta}^{(0)} A_w \quad (29)$$

where $W_\pi(\ell)$ and $\Sigma(\ell) = \Sigma_{\alpha\beta} + \Delta\Sigma(\ell)$ are the binding potential function and effective position-dependent stiffness, respectively. Within the DP approximation,

$$W_\pi^{(0)}(\ell) = w_{10}^{(0)} e^{-\kappa\ell} + w_{20}^{(0)} e^{-2\kappa\ell} + \dots \quad (30)$$

and

$$\Delta\Sigma^{(0)}(\ell) = s_{10}^{(0)} e^{-\kappa\ell} + s_{21}^{(0)} \kappa\ell e^{-2\kappa\ell} + \dots \quad (31)$$

and are identical to the findings of Fisher and Jin [4, 5], who derived the small gradient (local) limit (29) directly. The coefficients appearing in these expressions are determined by the coefficients of the binding potential functional. Thus, we identify $w_{10}^{(0)} = s_{10}^{(0)} = a_1^{(0)}$ while $w_{20}^{(0)} = b_1^{(0)} + b_2^{(0)}$, and $s_{21}^{(0)} = -2b_1^{(0)}$. We now wish to see how the above results are altered when one goes beyond the DP approximation.

3. Feynman–Hellman theorem and perturbation theory

Let us suppose that our microscopic model $H[m]$ can be written

$$H[m] = H^{(0)}[m] + \epsilon H^{(1)}[m] \quad (32)$$

containing a dimensionless field ϵ , which will later act as a small parameter. The reference Hamiltonian is the DP model, while

$$H^{(1)}[m] = \int d\mathbf{r} \Delta\Phi^{(1)}(m) \quad (33)$$

accounts for cubic and quartic corrections obtained by writing

$$\Delta\phi(m) = \frac{\kappa^2 (|m| - m_0)^2}{2} + \epsilon \Delta\Phi^{(1)}(m) \quad (34)$$

with

$$\Delta\Phi^{(1)}(m) = \frac{\kappa^2}{2} \delta m^2 \left(\frac{\delta m}{m_0} + \frac{1}{4} \frac{\delta m^2}{m_0^2} \right). \quad (35)$$

Thus, the potential (34) interpolates between the DP model ($\epsilon = 0$) and the ‘ m^4 ’ model ($\epsilon = 1$). Recall that the interfacial model is identified by evaluating $H[m]$ at the constrained magnetization m_Ξ . Taking the derivative of the constrained Hamiltonian

$$\frac{dH[m_\Xi]}{d\epsilon} = H^{(1)}[m_\Xi] + \int d\mathbf{r} \left. \frac{\delta H}{\delta m} \right|_{m_\Xi} \frac{dm_\Xi}{d\epsilon} \quad (36)$$

which, by virtue of the variational condition (12), leads to the familiar expression

$$\frac{dH[m_\Xi]}{d\epsilon} = \int d\mathbf{r} \Delta\Phi^{(1)}(m_\Xi), \quad (37)$$

similar to the well known Feynman–Hellman theorem in standard quantum mechanics. Note that the functional on the RHS depends on the full (ϵ -dependent) constrained magnetization and is a convenient means of formulating a perturbation expansion

$$H[m_\Xi] = H^{(0)}[m_\Xi^{(0)}] + \epsilon \tilde{H}^{(1)} + \epsilon^2 \tilde{H}^{(2)} + \dots \quad (38)$$

From this, it is straightforward to determine the corresponding expansion for the binding potential functional

$$W[\ell, \psi] = W^{(0)}[\ell, \psi] + \epsilon W^{(1)}[\ell, \psi] + \epsilon^2 W^{(2)}[\ell, \psi] + \dots \quad (39)$$

where the leading-order term is the DP result (22). In addition, we will also be able to compute expansions for the free interface $H_{\alpha\beta}[\ell]$ and the excess free energy of the wall– β interface $F_{w\beta}[\psi]$.

To determine the first-order and second-order perturbation functionals $\tilde{H}^{(1)}$ and $\tilde{H}^{(2)}$, we return to the Euler–Lagrange equation for the constrained profile

$$\nabla^2 \delta m_\Xi = \kappa^2 \delta m_\Xi + \epsilon \frac{\partial \Delta\Phi^{(1)}(m_\Xi)}{\partial m} \quad (40)$$

and seek a perturbative solution

$$\delta m_\Xi(\mathbf{r}; \epsilon) = \delta m_\Xi^{(0)}(\mathbf{r}) + \epsilon \delta m_\Xi^{(1)}(\mathbf{r}) + \dots \quad (41)$$

By definition, the leading-order term is the DP result, which satisfies the Helmholtz equation (13), while the first-order correction satisfies the inhomogeneous PDE

$$\nabla^2 \delta m_\Xi^{(1)} = \kappa^2 \delta m_\Xi^{(1)} + \frac{\partial \Delta\Phi^{(1)}(m_\Xi^{(0)})}{\partial m} \quad (42)$$

and vanishes at the interface, the wall, and infinity. Combining these, we obtain

$$\tilde{H}^{(1)}[\ell, \psi] = \int d\mathbf{r} \Delta\Phi^{(1)}(m_\Xi^{(0)}) \quad (43)$$

and

$$\tilde{H}^{(2)}[\ell, \psi] = \frac{1}{2} \int d\mathbf{r} \delta m_\Xi^{(1)} \frac{\partial \Delta\Phi^{(1)}(m_\Xi^{(0)})}{\partial m}. \quad (44)$$

A simplifying feature of the first-order correction is that it only depends on the zeroth-order profile $m_\Xi^{(0)}$ as calculated within the DP approximation. We begin with such a calculation for some preliminary quantities.

4. First-order perturbation theory for the free Hamiltonian

Consider a free but constrained configuration of the $\alpha|\beta$ interface. That is, the interface is infinitely far from any confining wall but the magnetization is constrained to be zero along a surface at height $\ell(\mathbf{x})$. Bulk phases α and β lie above and below the interface respectively. The interface partitions the system into two regions whose order-parameter fluctuations are shielded from each other, by virtue of the crossing criterion. The zeroth-order DP expressions for the position-dependent magnetizations in these regions are

$$m_{\Xi}^{(0)}(\mathbf{r}) = -m_0 + m_0 \text{---} \text{---} \text{---} \quad (45)$$

and

$$m_{\Xi}^{(0)}(\mathbf{r}) = m_0 - m_0 \text{---} \text{---} \text{---} \quad (46)$$

above and below the interface respectively. The first-order result for the free interfacial Hamiltonian is

$$H_{\alpha\beta}[\ell] = H_{\alpha\beta}^{(0)}[\ell] + \epsilon \int d\mathbf{r} \Delta \Phi^{(1)}(m_{\Xi}^{(0)}) + \dots \quad (47)$$

where the first term is simply the zeroth-order DP result $H_{\alpha\beta}^{(0)}[\ell] = \Sigma_{\alpha\beta}^{(0)} A_{\alpha\beta}$. Hence,

$$H_{\alpha\beta}[\ell] = \Sigma_{\alpha\beta}^{(0)} A_{\alpha\beta} + \epsilon \kappa m_0^2 \left\{ -\frac{1}{2} \text{---} \text{---} \text{---} - \frac{1}{2} \text{---} \text{---} \text{---} + \frac{1}{8} \text{---} \text{---} \text{---} + \frac{1}{8} \text{---} \text{---} \text{---} \right\} \quad (48)$$

where we have expressed the results diagrammatically. The single wavy line represents the free interface while the thick straight lines denote the Green's function K . The diagrams appearing in this formula are all of the same type and have $n = 3, 4$ (black) dots on the interface and one (black) dot either above or below the surface. They correspond to multi-dimensional integrals. For example,

$$\text{---} \text{---} \text{---} = \kappa \int_{V_+} d\mathbf{r} \left\{ \int ds_{\ell} K(\mathbf{r}_{\ell}, \mathbf{r}) \right\}^4 \quad (49)$$

where, in general, the integrand contains n kernels K connecting a point off the interface to n different points on it. Black dots on the surface have the same interpretation as before—one must integrate over all points on the surface with the appropriate area element. A black point off the surface means that one must integrate over the appropriate semi-volume V_+ (here above the interface) together with a multiplicative factor of κ . The latter is introduced so that the diagram has the dimensions of area. Again, each kernel may be thought of as representing a short tube-like fluctuation protruding from the surface, only a few bulk correlation lengths long (since the kernel decays exponentially quickly). Such fluctuations can be thought of as giving the interface a 'corona'. As we shall show, these shift the DP expression for the surface tension and also introduce curvature corrections. To see this, consider first the case of a planar interface of (infinite) area $A_{\alpha\beta}$. By definition, the value of the Hamiltonian per unit area is equal to the surface tension, so we can identify

$$\Sigma_{\alpha\beta}(\epsilon) = \Sigma_{\alpha\beta}^{(0)} + \frac{\kappa m_0^2 \epsilon}{A_{\alpha\beta}} \left\{ -\text{---} \text{---} \text{---} + \frac{1}{4} \text{---} \text{---} \text{---} \right\}. \quad (50)$$

The integrals are easily performed

$$\text{---} \text{---} \text{---} = \frac{A_{\alpha\beta}}{3} \quad \text{---} \text{---} \text{---} = \frac{A_{\alpha\beta}}{4} \quad (51)$$

which implies the tension is shifted to

$$\Sigma_{\alpha\beta}(\epsilon) = \kappa m_0^2 \left\{ 1 + \epsilon \left(-\frac{1}{3} + \frac{1}{16} \right) + \dots \right\} \quad (52)$$

where we have highlighted the different numerical contributions for the cubic and quartic perturbations. Setting $\epsilon = 1$, we find $\Sigma_{\alpha\beta} \approx 0.72 \kappa m_0^2$, which is in much better agreement with the mean-field expression $\Sigma_{\alpha\beta} = (2/3)\kappa m_0^2$ of the full ‘ m^4 ’ theory [19]. Thus, the dominant numerical correction to the DP expression for the surface tension arises from the cubic term in $\Delta\phi^{(1)}$ and is accurately accounted for by first-order perturbation theory. This point is further amplified by calculating exactly the mean-field surface tension $\Sigma_{\alpha\beta}(\epsilon)$ for the potential (34):

$$\frac{\Sigma_{\alpha\beta}(\epsilon)}{\kappa m_0^2} = \left(\frac{4}{3\epsilon} - 2\right) \left(\sqrt{4 - 3\epsilon} - 2\right) + \frac{4(1 - \epsilon)}{\sqrt{\epsilon}} \ln \frac{2(1 + \sqrt{\epsilon})}{\sqrt{4 - 3\epsilon} + \sqrt{\epsilon}}. \quad (53)$$

It is straightforward to check that this is consistent with the limiting cases at $\epsilon = 1$ and 0 respectively, and also reproduces the perturbation expansion (52). While this function looks rather ominous, it is almost linear in character over the required domain.

In addition to correcting the value of the surface tension, the ‘corona’ diagrams lead to curvature terms, which reveal the more general structure of the free Hamiltonian. To appreciate this, consider the case of an undulating interfacial profile. Provided the local principal radii of curvature $R_1^\ell(\mathbf{x})$ and $R_2^\ell(\mathbf{x})$, are always large, one can expand the integrals to find

$$H_{\alpha\beta}[\ell] = \int ds_\ell \left\{ \Sigma_{\alpha\beta} + \frac{\kappa_{\alpha\beta}}{2} \left(\frac{1}{R_1^\ell} + \frac{1}{R_2^\ell} \right)^2 + \frac{\bar{\kappa}_{\alpha\beta}}{R_1^\ell R_2^\ell} + \dots \right\} \quad (54)$$

where $\kappa_{\alpha\beta} = \epsilon m_0^2 / 64\kappa$ and $\bar{\kappa}_{\alpha\beta} = -\epsilon m_0^2 / 128\kappa$ are the bending rigidity and saddle-splay coefficients of the square mean curvature and Gaussian curvature, respectively [20, 21]. The notation here is similar to that adopted by Blokhuis and Bedeaux [21], although we have added a subscript to try to avoid confusion with the inverse bulk correlation length. Note there is no term proportional to the mean curvature as required by the Ising symmetry.

A similar calculation reveals the general structure of the wall- β interfacial free energy. Consider the interface between a wall described by the height function $\psi(\mathbf{x})$ and the bulk β phase corresponding to spontaneous magnetization m_0 . Recall that the magnetization at the surface m_1 is positive so that this interface does not exhibit any wetting behaviour. The DP result, equation (28), for the excess free energy involves only the area and local mean curvature of the wall. No higher order curvature corrections are present. Beyond the DP approximation, we may reasonably expect this to change with the cubic and quartic interactions, giving rise to additional curvature contributions. The perturbation theory is very similar to that described for the free interface and, to first order, we find

$$F_{w\beta}[\psi] = F_{w\beta}^{(0)}[\psi] + \epsilon \frac{\kappa m_0^2}{2} \left\{ t^3 \text{[diagram]} + \frac{t^4}{4} \text{[diagram]} \right\} + \dots \quad (55)$$

where this time the wavy line denotes the shape of the bounding wall. The diagrams are easily evaluated as an expansion in the inverse principal radii of curvature at the wall, and we find

$$F_{w\beta}[\psi] = \int ds_\psi \left\{ \Sigma_{w\beta} + C_{w\beta} \left(\frac{1}{R_1^\psi} + \frac{1}{R_2^\psi} \right) + \frac{\kappa_{w\beta}}{2} \left(\frac{1}{R_1^\psi} + \frac{1}{R_2^\psi} \right)^2 + \frac{\bar{\kappa}_{w\beta}}{R_1^\psi R_2^\psi} + \dots \right\} \quad (56)$$

where the ellipses denote higher-order terms in the curvature. The new surface tension $\Sigma_{w\beta}$ and bending rigidity coefficient $C_{w\beta}$ contain very small corrections of order $\mathcal{O}(\epsilon t^3)$ to the DP results quoted earlier. The new rigidities $\kappa_{w\beta} \sim \bar{\kappa}_{w\beta}$ are $\mathcal{O}(\epsilon t^3)$ and are considerably smaller in magnitude than $C_{w\beta}$.

Note that the expression for the free energy $F_{w\beta}$, for the present m^4 -theory contains higher-order inverse powers of the local radii of curvature. This appears to rule out the morphological hypothesis of König *et al* [22], which suggests that the series truncates. Interestingly, however, truncation does occur at DP level where $\kappa_{w\beta}$ and higher coefficients are all zero.

5. First-order perturbation theory for $W[\ell, \psi]$

5.1. General equations

To begin, we restate the perturbation theory for the bulk potential in a slightly more general way. The calculation of the non-local binding potential only requires us to specify the form of the bulk potential in the wetting layer region where $m > 0$. We write

$$\Delta\phi(m) = \frac{\kappa^2 \delta m^2}{2} + \sum_{n=3}^{\infty} \epsilon_n \kappa^2 m_0^{2-n} \delta m^n \quad (57)$$

where $\delta m = m - m_0$ and the ϵ_n are all dimensionless parameters. Thus, the usual ‘ m^4 ’ theory corresponds to $\epsilon_3 = \frac{1}{2}$, $\epsilon_4 = \frac{1}{8}$ and $\epsilon_n = 0$ for $n > 4$. To first order in perturbation theory, all the contributions are additive and we seek to write the non-local binding potential functional

$$W[\ell, \psi] = W^{(0)}[\ell, \psi] + \sum_{n=3}^{\infty} \epsilon_n W_n^{(1)}[\ell, \psi] + \dots \quad (58)$$

where, in an obvious notation, the $W_n^{(1)}$ are the perturbations corresponding to the term δm^n in the bulk potential. To determine these, it is convenient to order the expansion of $\delta m_{\Xi}^{(0)}$ in the number of tubes that span the interfaces

$$\begin{aligned} \delta m_{\Xi}^{(0)} = & \left(\delta m_1 \overbrace{\text{---}}^{\text{---}} - m_0 \overbrace{\text{---}}^{\text{---}} \right) - \left(\delta m_1 \overbrace{\text{---}}^{\text{---}} - m_0 \overbrace{\text{---}}^{\text{---}} \right) \\ & + \left(\delta m_1 \overbrace{\text{---}}^{\text{---}} - m_0 \overbrace{\text{---}}^{\text{---}} \right) - \dots \end{aligned} \quad (59)$$

From (43), it follows that the first-order perturbations are given by

$$W_n^{(1)}[\ell, \psi] = \kappa^2 m_0^{2-n} \int_{V_{\beta}} d\mathbf{r} \left(\delta m_{\Xi}^{(0)} \right)^n - A_n^{(1)}[\ell] - B_n^{(1)}[\psi] \quad (60)$$

where V_{β} denotes the volume of the wetting layer between the wall and interface. The functionals $A[\ell]$ and $B[\psi]$ do not describe interactions between the interface and wall and are introduced so that W vanishes for infinite separation. For example,

$$A_4^{(1)}[\ell] = (-1)^4 \kappa m_0^2 \overbrace{\text{---}}^{\text{---}} \quad (61)$$

$$B_4^{(1)}[\psi] = \kappa m_0^2 t^4 \overbrace{\text{---}}^{\text{---}} \quad (62)$$

where, in each case, the wavy line denotes a configuration of the surface that corresponds to the argument of the functional. All that remains now is the evaluation of the integrals and the classification and simplification of the ensuing wetting diagrams.

5.2. Wetting diagrams for cubic and quartic interactions

Substituting the magnetization profile into the first-order perturbation expression (60) for $n = 3$ and 4 leads to the following expressions for the first-order cubic and quartic corrections to the DP functional:

$$\begin{aligned} \frac{W_3^{(1)}}{\kappa m_0^2} = & 3t \left(\overbrace{\text{---}}^{\text{---}} - \overbrace{\text{---}}^{\text{---}} \right) - 3t^2 \left(\overbrace{\text{---}}^{\text{---}} - \overbrace{\text{---}}^{\text{---}} \right) + 3 \left(\overbrace{\text{---}}^{\text{---}} - \overbrace{\text{---}}^{\text{---}} \right) \\ & - 3t^3 \left(\overbrace{\text{---}}^{\text{---}} - \overbrace{\text{---}}^{\text{---}} \right) + 3t \left(\overbrace{\text{---}}^{\text{---}} - 2 \overbrace{\text{---}}^{\text{---}} \right) - 3t^2 \left(\overbrace{\text{---}}^{\text{---}} - 2 \overbrace{\text{---}}^{\text{---}} \right) \end{aligned} \quad (63)$$

and

$$\begin{aligned} \frac{W_4^{(1)}}{\kappa m_0^2} = & -4t \left(\text{Diagram 1} - \text{Diagram 2} \right) - 4t^3 \left(\text{Diagram 3} - \text{Diagram 4} \right) - 4 \left(\text{Diagram 5} - \text{Diagram 6} \right) \\ & - 4t^4 \left(\text{Diagram 7} - \text{Diagram 8} \right) + 6t^2 \left(\text{Diagram 9} - 2 \text{Diagram 10} \right) + 6t^2 \left(\text{Diagram 11} - 2 \text{Diagram 12} \right) \\ & + 6t^2 \text{Diagram 13}. \end{aligned} \tag{64}$$

Higher-order diagrams exist but involve at least three tubes that span the surfaces and would generate terms of order $\mathcal{O}(e^{-3\kappa\ell})$ in the standard binding potential function. Each of the new wetting diagrams has one black dot lying between the surfaces and represents an integral over the volume V_β of the wetting layer. The associated infinitesimal measure is $\kappa d\mathbf{r}$. Thus, the first wetting diagram in the expansion of $W_3^{(1)}$ is

$$\text{Diagram 1} = \kappa \int ds_\psi \int_{V_\beta} d\mathbf{r} K(\mathbf{r}_\psi, \mathbf{r}) \left\{ \int ds_\ell K(\mathbf{r}, \mathbf{r}_\ell) \right\}^2 \tag{65}$$

where we have labelled the points in an obvious notation. It is natural to interpret this as a *splitting* of a tube-like fluctuation connecting the surfaces. The second diagram in the same cubic interaction does not involve a splitting but instead adds a ‘corona’ corresponding to short tube-like fluctuations away from the interface:

$$\text{Diagram 2} = \kappa \int \int \int_{V_\beta} ds_\psi ds'_\ell d\mathbf{r} K(\mathbf{r}_\psi, \mathbf{r}'_\ell) K(\mathbf{r}'_\ell, \mathbf{r}) \left\{ \int ds_\ell K(\mathbf{r}, \mathbf{r}_\ell) \right\}^2. \tag{66}$$

Similar interpretations apply to all the wetting diagrams. One contribution which is of particular novelty is the \mathcal{X} diagram

$$\text{Diagram 13} = \kappa \int \int \int \int_{V_\beta} ds_\psi ds'_\psi ds_\ell ds'_\ell d\mathbf{r} K(\mathbf{r}_\psi, \mathbf{r}) K(\mathbf{r}'_\psi, \mathbf{r}) K(\mathbf{r}, \mathbf{r}_\ell) K(\mathbf{r}, \mathbf{r}'_\ell) \tag{67}$$

and arises from the quartic interaction. This has an appealing physical interpretation as a local pinching of two tubes that span the surfaces. As we shall see, this is a rather interesting diagram even though ultimately it does not influence the leading-order physics.

5.3. Wetting diagram relations

The cubic and quartic interactions appear to give rise to a plethora of new wetting diagrams. However, the physics represented by these perturbations is rather simple and can be elegantly expressed in a more concise fashion. The essential ingredients in this simplification are various relations between the wetting diagrams which express their reducibility. We will illustrate this with some examples.

Consider the first wetting diagram appearing in $W_3^{(1)}$. To begin, suppose that the wetting layer has planar area A_w and is of constant thickness ℓ . The integrals are easily evaluated, yielding

$$\text{Diagram 1} = A_w (e^{-\kappa\ell} - e^{-2\kappa\ell}). \tag{68}$$

This can be expressed diagrammatically

$$\text{Diagram 1} = \text{Diagram 3} - \text{Diagram 4} \tag{69}$$

showing that the perturbative diagram is reducible to the DP contributions Ω_1^1 and Ω_1^2 . The net effect of this diagram is, therefore, to simply shift the coefficients

$$a_1^{(0)} \rightarrow a_1 = a_1^{(0)} + 3\epsilon_3 t \kappa m_0^2 \tag{70}$$

$$b_1^{(0)} \rightarrow b_1 = b_1^{(0)} - 3\epsilon_3 t \kappa m_0^2 \tag{71}$$

appearing in the DP expression for W . Moreover, a nice feature of the perturbation theory is that there is no need to keep precise book-keeping concerning such shifts. This can be done exactly at the end of the calculation once the general diagrammatic structure has been elucidated.

The above expression is not quite the whole relation for the wetting diagram since interfacial and substrate curvature are not allowed for. More generally, one finds (after a few integrations)

$$\text{Diagram with black triangle} = \text{Diagram with two tubes} + \frac{1}{2} \text{Diagram with one tube} - \text{Diagram with one tube and black triangle} + \dots \quad (72)$$

where we have introduced a new type of diagram containing a black triangle. The triangle will always lie on a surface and is interpreted as an integral over the surface with local measure ds multiplied by the sum of the local principal curvatures, measured in units of κ (to preserve the units of the diagrams). Thus,

$$\text{Diagram with one tube and black triangle} = \frac{1}{\kappa} \int \int ds_\psi ds_\ell K(\mathbf{r}_\psi, \mathbf{r}_\ell) \left(\frac{1}{R_1^\ell} + \frac{1}{R_2^\ell} \right) \quad (73)$$

and similarly if a triangle is placed on the wall. The ellipses in the wetting diagram relation (72) denote higher-order curvature terms which are negligible.

Similarly, for the second wetting diagram in $W_3^{(1)}$, one can write the relation

$$\text{Diagram with two tubes and black triangle} = \frac{1}{3} \text{Diagram with two tubes} + \frac{1}{18} \text{Diagram with one tube and black triangle} + \dots \quad (74)$$

where here the ellipses also include terms involving four tubes that span the surfaces as well as higher-order curvatures. The same process is also valid for diagrams with two tubes spanning the surfaces. For example

$$\text{Diagram with two tubes and black triangle} = \frac{1}{3} \text{Diagram with two tubes and black triangle} + \dots \quad (75)$$

Again the effect of these diagrams is to shift the coefficient of the Ω_1^2 diagram and add negligible curvature terms. In the first-order perturbation theory all bar one diagram can be recast as a sum of the DP diagrams Ω_1^1 , Ω_1^2 and Ω_2^1 together with curvature corrections. The only contribution for which there is no such relation is the \mathcal{X} diagram describing the two-tube pinching process (67), which is not reducible. However, relations involving it do emerge at second order in perturbation theory.

In summary, three effects emerge at first order in perturbation theory: (1) rescaling of the coefficients a_1 , b_1 etc, (2) appearance of curvature corrections and (3) introduction of non-zigzag diagrams describing tube interactions.

6. Second-order perturbation theory for W

At second order, by far the most important contribution arises from the cubic interaction in $\Delta\Phi^{(1)}$. Contributions of order ϵ_4^2 , as well as mixing terms $\epsilon_3\epsilon_4$, are small and do not introduce any new physics. For ease of presentation, we suppose that the potential perturbation has only one power, $\Delta\Phi^{(1)} = \kappa^2 m_0^{2-n} \delta m^n$, and determine the second-order term in

$$W[\ell, \psi] = W^{(0)}[\ell, \psi] + \epsilon_n W^{(1)}[\ell, \psi] + \epsilon_n^2 W^{(2)}[\ell, \psi]. \quad (76)$$

Setting $n = 3$ at the end of the calculation reveals the dominance of the cubic interaction at this order. The second-order perturbation is

$$W^{(2)}[\ell, \psi] = \frac{n \kappa^2 m_0^{2-n}}{2} \int d\mathbf{r} \delta m_\Xi^{(1)} (\delta m_\Xi^{(0)})^{n-1} - A_n^{(2)}[\ell] - B_n^{(2)}[\psi] \quad (77)$$

where, as in the first-order perturbation theory, functionals $A_n^{(2)}[\ell]$ and $B_n^{(2)}[\psi]$ are introduced so that, by construction, $W^{(2)}$ vanishes when the interface is delocalized from the wall. They need not be specified explicitly, as they are automatically generated by the integral in (77).

The second-order term in the potential W depends on the first-order correction to the profile $\delta m_{\Xi}^{(1)}$, which satisfies

$$\nabla^2 \delta m_{\Xi}^{(1)} = \kappa^2 \delta m_{\Xi}^{(1)} + n \kappa^2 m_0^{2-n} (\delta m_{\Xi}^{(0)})^{n-1}. \tag{78}$$

Substitution of the DP profile leads to the PDE

$$\nabla^2 \delta m_{\Xi}^{(1)} = \kappa^2 \delta m_{\Xi}^{(1)} - n(-1)^n \kappa^2 m_0 \times \left\{ (n-1)t \left(\text{Diagram 1} - \text{Diagram 2} \right) + \text{Diagram 3} + (n-1) \left(\text{Diagram 4} - \text{Diagram 5} \right) \right\} \tag{79}$$

where we have curtailed the expansion at two tubes spanning the surfaces, and neglected terms of $\mathcal{O}(t^2)$. The inhomogeneous PDE can be solved in a standard manner using the same Green's function $K(\mathbf{r}_1, \mathbf{r}_2)$. Thus, the solution can also be written diagrammatically and, after some algebra, we find

$$\delta m_{\Xi}^{(1)} = \frac{(-1)^n n}{2} \left\{ (n-1) \delta m_1 \left[\left(\text{Diagram 1} - \text{Diagram 2} \right) - \left(\text{Diagram 3} - \text{Diagram 4} \right) \right] + m_0 \left[\left(\text{Diagram 5} - \text{Diagram 6} \right) + \left(\text{Diagram 7} - \text{Diagram 8} \right) - \left(\text{Diagram 9} - \text{Diagram 10} \right) \right] + (n-1) \left(\text{Diagram 11} - \text{Diagram 12} \right) - (n-1) \left(\text{Diagram 13} - \text{Diagram 14} \right) \right\}. \tag{80}$$

Specializing in the dominant cubic interaction ($n = 3$), we find for the second-order perturbation in W

$$\frac{W_3^{(2)}[\ell, \psi]}{\kappa m_0^2} = -\frac{9}{4} \{ 4t D_1^1 + D_1^2 \} + \mathcal{O}(t^2) \tag{81}$$

where D_1^1 and D_1^2 denote the following sum of diagrams:

$$D_1^1 = \text{Diagram 1} - \text{Diagram 2} - \text{Diagram 3} + \text{Diagram 4} \tag{82}$$

and

$$D_1^2 = 2 \text{Diagram 5} - \text{Diagram 6} - \text{Diagram 7} + 4 \text{Diagram 8} - 4 \text{Diagram 9} + 4 \text{Diagram 10} - 4 \text{Diagram 11}. \tag{83}$$

These diagrams determine the rescaling of the coefficients a_1 and b_1 , and also generate curvature corrections due to the interface. Again, the key to understanding their net effect is through wetting diagram relations. For example, the following quartic diagram can be expressed:

$$\text{Diagram 12} = \frac{1}{3} \text{Diagram 13} + \frac{2}{9} \text{Diagram 14} + \dots \tag{84}$$

where the ellipses include higher-order interfacial curvature terms and four-tube diagrams. In this way, each of the contributions in (81) can be written as a sum of the diagrams

$$\text{Diagram 13}, \quad \text{Diagram 14}, \quad \text{Diagram 15} \tag{85}$$

similar to the first-order perturbation theory. If one extends the calculation to allow terms of order t^2, t^3 etc, one also encounters wetting diagrams where corona-like tubes emanate from

the substrate. These are, in fact, the same as the diagrams in D_1^1 and D_1^2 but with the interfacial and substrate surfaces switched. Thus, for example,


(86)

has a coefficient proportional to t^3 and will add higher-order powers of t in the expansion of a_1 , and also generate curvature corrections due to the substrate which can be recast in terms of the diagram

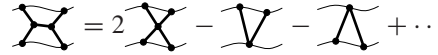
$$\mathcal{I} = \frac{1}{\kappa} \int \int ds_\psi ds_\ell K(r_\psi, r_\ell) \left(\frac{1}{R_1^\psi} + \frac{1}{R_2^\psi} \right). \quad (87)$$

Again, the general structure obtained from the first-order perturbation theory is unchanged.

Working to $\mathcal{O}(t^2)$, one also generates wetting diagrams which are closely related to the two-tube pinching process which arose in the first-order perturbation from the quartic interaction. For example,


(88)

whose coefficient is proportional to t^2 . The two central black dots in the wetting layer are connected by a tube-like fluctuation which does not attach to either the wall or the interface. The connecting tube is necessarily of short length because the corresponding integral is heavily damped by the kernel K . This is neatly expressed diagrammatically,


(89)

leading to the rescaling of the coefficients of Ω_1^2 , Ω_2^1 and \mathcal{X} . Curvature corrections, represented by the ellipsis, are of negligible importance for two-tube diagrams.

In summary, second-order perturbation theory leads to the same three effects as highlighted in the first-order calculation: the rescaling of coefficients and the appearance of curvature and tube-interaction diagrams.

7. The general structure of the non-local binding potential

The general structure of the non-local binding potential functional for short-ranged wetting is now apparent. Up to ‘two tubes’, the functional has an asymptotic large-distance decay described by the diagrams

$$W = a_1 \mathcal{I} + c_1 \mathcal{A} + c_2 \mathcal{J} + b_1 \mathcal{V} + b_2 \mathcal{T} + d_1 \mathcal{X} + \dots \quad (90)$$

which should be compared with the DP result (27). Thus, going beyond DP generates curvature terms (shown for one-tube diagrams only) and also a tube-interaction diagram. The corresponding algebraic expressions are given by equations (24), (73), (87), (25), (26) and (67). The coefficients are geometry independent and all have power series expansions in the scaling field t . The leading-order behaviours are

$$\begin{aligned} \frac{a_1}{\kappa m_0^2} &= \alpha t, & \frac{b_1}{\kappa m_0^2} &= \beta, & \frac{b_2}{\kappa m_0^2} &= \beta t^2, \\ \frac{c_1}{\kappa m_0^2} &= \gamma t, & \frac{c_2}{\kappa m_0^2} &= \gamma t^2, & \frac{d_1}{\kappa m_0^2} &= \chi t^2 \end{aligned} \quad (91)$$

and are specified by just four dimensionless constants reflecting the surface exchange symmetry of W . The coefficients b_2 , c_2 and d_1 all vanish as t^2 , implying that the associated diagrams are

of negligible importance at critical wetting. The second diagram, describing the curvature correction due to the $\alpha|\beta$ interface, is necessarily much smaller than Ω_1^1 and is therefore also negligible, given that c_1 also vanishes at the critical wetting phase boundary. Thus, the diagrammatic expression for W is the same as calculated using the DP approximation in [1] but with different numerical coefficients. This is the main finding of our study.

The exact values of the above coefficients can be calculated for the ‘ m^4 ’ LGW potential (4), by matching with mean-field results for specific interfacial and wall configurations. Consider for example the simplest situation of a flat wall, $\psi = 0$ and a flat interface $\ell(\mathbf{x}) = \ell$. The corresponding planar binding potential function is defined as

$$W_\pi(\ell) = \frac{W[\ell, 0]}{A_w} \Big|_{\ell(\mathbf{x})=\ell} \quad (92)$$

and can be identified with the diagrams

$$A_w W_\pi(\ell) = a_1 \overline{\text{---}} + b_1 \overline{\text{---}} + b_2 \overline{\text{---}} + d_1 \overline{\text{---}} + \dots \quad (93)$$

The first three diagrams are of DP type and were discussed in [1]. The new diagram can also be evaluated exactly

$$\overline{\text{---}} = A_w \kappa \ell e^{-2\kappa\ell} \quad (94)$$

implying that there are non-purely-exponential terms in the binding potential. Thus, the binding potential function necessarily has the general expansion

$$W_\pi(\ell) = a_1 e^{-\kappa\ell} + (b_1 + b_2 + d_1 \kappa \ell) e^{-2\kappa\ell} + \dots \quad (95)$$

with coefficients specified in (91). This is identical to the findings of Fisher and Jin, who calculated $W_\pi(\ell)$ directly [5]. One advantage of the Green’s function approach is that the diagram leading to the non-purely-exponential term is isolated and can be evaluated for other geometries. For example, for spherical interfacial and wall shapes

$$\overline{\text{---}} = \sqrt{A_w A_{\alpha\beta}} \kappa \ell e^{-2\kappa\ell} \quad (96)$$

where, as in [1], $A_w = 4\pi R^2$ and $A_{\alpha\beta} = 4\pi (R + \ell)^2$ are the areas of the wall and interfacial configurations, respectively.

We can now determine the coefficients a_1, b_1, \dots by comparing (95) with the known asymptotic decay of W_π for arbitrary potentials $\Delta\Phi(m)$. This can be calculated independently without recourse to perturbation theory. For planar interfacial and wall configurations, the constrained profile $m_\Xi \equiv m_\pi(z; \ell)$ satisfies the ‘energy-conservation’ condition

$$\frac{1}{2} \left(\frac{\partial m_\pi}{\partial z} \right)^2 = \Delta\phi(m_\pi) - W'_\pi(\ell). \quad (97)$$

This can be integrated, and the large-distance expansion exactly determined. For the ‘ m^4 ’ potential (4), we find

$$\begin{aligned} \frac{a_1}{\kappa m_0^2} &= 4t, & \frac{b_1}{\kappa m_0^2} &= 4 \\ \frac{b_2}{\kappa m_0^2} &= 4t^2, & \frac{d_1}{\kappa m_0^2} &= 6t^2. \end{aligned} \quad (98)$$

The curvature coefficient $\gamma = -8$ can be determined in a similar fashion by considering spherical wall and interfacial configurations.

One can go further in this analysis and determine the coefficients for the perturbative potential (34) to all orders in ϵ . We only quote the results for a_1 and b_1

$$\frac{a_1}{\kappa m_0^2} = \frac{8t}{2 - \epsilon + \sqrt{4 - 3\epsilon}}, \quad \frac{b_1}{\kappa m_0^2} = \frac{16}{(2 - \epsilon + \sqrt{4 - 3\epsilon})^2} \quad (99)$$

which smoothly interpolate between the DP and ‘ m^4 ’ theory results.

8. Non-local model for wetting at planar substrates

In this section, we show how all the wetting diagrams appearing in the asymptotic expansion (90) simplify when the substrate is planar ($\psi = 0$). Clearly, there is no contribution from substrate curvature and we write the interfacial model

$$H[\ell] = H_{\alpha\beta}[\ell] + W[\ell] \quad (100)$$

with planar binding potential functional ($W[\ell] \equiv W[\ell, 0]$)

$$W[\ell] = a_1 \overline{\mathcal{I}} + c_1 \overline{\mathcal{I}}^c + b_1 \overline{\mathcal{V}} + b_2 \overline{\mathcal{A}} + d_1 \overline{\mathcal{X}} + \dots \quad (101)$$

containing two new diagrams compared with the corresponding DP expression. Three of these diagrams can be evaluated by simply holding the dot (or triangle) on the upper interface fixed and integrating over the wall:

$$\overline{\mathcal{I}} = \int d\mathbf{x} \sqrt{1 + (\nabla\ell)^2} e^{-\kappa\ell}, \quad (102)$$

$$\overline{\mathcal{I}}^c = \int d\mathbf{x} \sqrt{1 + (\nabla\ell)^2} \left(\frac{1}{R_1^\ell} + \frac{1}{R_2^\ell} \right) e^{-\kappa\ell} \quad (103)$$

and

$$\overline{\mathcal{A}} = \int d\mathbf{x} \sqrt{1 + (\nabla\ell)^2} e^{-2\kappa\ell} \quad (104)$$

which are all local contributions to the effective Hamiltonian $H[\ell]$. In particular, if $\nabla\ell$ is small, one can see how each contributes towards a local binding potential function and/or effective position-dependent stiffness. Note that, if the coefficient c_1 of the curvature diagram (103) is zero, as it is at DP level, the Ω_1^1 diagram (102) determines the leading-order exponential decays of $W_\pi(\ell)$ and $\Sigma(\ell)$. Beyond DP, however, the curvature diagram also contributes to $\Sigma(\ell)$.

In contrast, the two remaining diagrams, Ω_1^2 and \mathcal{X} , are strongly non-local. As remarked in [7] application of the convolution theorem reduces the triple integral (25) to a double integral

$$\overline{\mathcal{V}} = \int \int d\mathbf{s}_1 d\mathbf{s}_2 e^{-\kappa\ell(\mathbf{x}_1)} S(x_{12}; \bar{\ell}_{12}) e^{-\kappa\ell(\mathbf{x}_2)} \quad (105)$$

where $\bar{\ell}_{12} = (\ell(\mathbf{x}_1) + \ell(\mathbf{x}_2))/2$ is the mean interfacial height of the two points at the interface. Here S is a two-body interfacial interaction which decays as a two-dimensional Gaussian

$$S(x_{12}; \ell) \approx \frac{\kappa}{4\pi\ell} \exp\left(-\frac{\kappa x_{12}^2}{4\ell}\right) \quad (106)$$

and which controls the repulsion of the interface from the wall. By construction, the integrated strength of S is unity. There are two features about this effective many-body interaction which are worth commenting on. Firstly, its range increases as the square root of the film thickness and, therefore, becomes longer ranged as the interface unbinds. It is this that necessitates a non-local treatment of short-ranged critical wetting, and is responsible for the breakdown of

local theories. Also, the same Gaussian interaction (106) follows from a simple saddle-point evaluation of the integral (25) over the wall. This means that the interaction between two fixed points on the interface arises due to a connecting tube that reflects off the wall and is of minimal length. This physical interpretation will be useful in discussions of wetting at non-planar walls, where an exact convolution evaluation of Ω_1^2 is not available.

Similar arguments apply to the \mathcal{X} diagram describing the two-tube interaction, which can be written

$$\overline{\mathcal{X}} = \int \int d\mathbf{s}_1 d\mathbf{s}_2 e^{-\kappa\ell(\mathbf{x}_1)} X(x_{12}; \bar{\ell}_{12}) e^{-\kappa\ell(\mathbf{x}_2)}. \quad (107)$$

The two-body interaction describing this interaction also depends on the mean interfacial height only, and is given by

$$X(x; \ell) = \frac{\kappa^2}{4\pi} \Gamma\left(0, \frac{\kappa x^2}{4\ell}\right) \quad (108)$$

where $\Gamma(0, z)$ is the incomplete gamma function. At large distances, this decays similarly to the two-dimensional Gaussian (106).

Finally, we mention that in the strict small-gradient limit the non-local Hamiltonian reduces to

$$H[\ell] = \int d\mathbf{x} \left\{ \frac{\Sigma(\ell)}{2} (\nabla\ell)^2 + W_\pi(\ell) \right\} + \Sigma_{\alpha\beta} A_w \quad (109)$$

where the position dependent contributions to the binding potential and stiffness coefficient have the general decays

$$W(\ell) = w_{10} e^{-\kappa\ell} + (w_{21}\kappa\ell + w_{20}) e^{-2\kappa\ell} + \dots \quad (110)$$

and

$$\Delta\Sigma(\ell) = s_{10} e^{-\kappa\ell} + (s_{22}\kappa^2\ell^2 + s_{21}\kappa\ell + s_{20}) e^{-2\kappa\ell} + \dots \quad (111)$$

respectively. All seven coefficients exhibit power-law dependences on the scaling field t and are determined by the five coefficients a_1, b_1, c_1, b_2 and d_1 . We find $w_{10} \sim s_{10} \sim t$, $w_{21} \sim s_{22} \sim t^2$ and all other coefficients finite at $t = 0$. These are in precise agreement with the local theory of Jin and Fisher [4].

9. Discussion

In this paper, we have extended our earlier derivation of a non-local interfacial Hamiltonian for short-ranged wetting beyond the DP approximation. We have shown that the diagrammatic method introduced in our first paper combines rather nicely with perturbation theory and allows us to derive the general structure of the binding potential functional W . While this contains some new diagrams describing curvature corrections and tube interactions, these are of negligible importance for wetting. The dominant diagrammatic structure of W is the same as that derived for the DP model, albeit with slightly shifted coefficients. The values of these coefficients have been determined exactly. We also showed how all the diagrams in the asymptotic expansion of W (up to two tubes) simplify for wetting at planar substrates. While some local contributions are accurately described by a binding potential function and position-dependent stiffness, the non-local contributions generate weak long-ranged two-body interfacial interactions, which play a crucial role at critical wetting.

To finish our article, we make a number of remarks concerning the interpretation, limitations and further extension of the present approach:

9.1. New features

Going beyond the DP approximation alters the binding potential functional in three different ways: rescaling of the coefficients $a_1, b_1 \dots$, and the introduction of curvature and tube interaction diagrams. These effects could have been anticipated on very general grounds. Even for a free Hamiltonian, going beyond DP alters the surface tension and introduces Helfrich-like rigidity terms, consistent with morphological expectations. The first two effects merely mirror those in W . Also, there must be a mechanism which generates non-purely-exponential terms in the binding potential function $W_\pi(\ell)$ beyond DP. This is fulfilled by the two-tube interaction diagram \mathcal{X} .

9.2. Generalization of the LGW model

One could consider a slightly generalized LGW model in which the coefficient of $(\nabla m)^2$ is a function of the order parameter [19]. By expanding this function about m_0 , it is straightforward to show that the corresponding first-order perturbation corrections to W are equivalent to cubic, quartic etc corrections to the DP potential, which we have considered explicitly. The same is also true of square-Laplacian contributions to $H[m]$, which are equivalent to a shift in the value of κ plus the aforementioned cubic, quartic and higher-order corrections. In both cases, the diagrammatic structure of W remains unaltered to first order. Of course, this robustness is to be expected. As remarked at the end of our first paper, the form of W is necessitated by exact sum-rule requirements.

9.3. Coupling to a surface field and enhancement

While we have restricted ourselves to fixed boundary conditions at the wall, it is straightforward to extend the Green's function method to different kinds of surface boundary conditions. In particular, one may consider LGW models of the form [17]

$$H[m] = \int d\mathbf{r} \left\{ \frac{1}{2}(\nabla m)^2 + \Delta\phi(m) \right\} + \int d\mathbf{s}_\psi \phi_1(m(\mathbf{r}_\psi)) \quad (112)$$

where $\phi_1(m) = -\frac{g}{2}m^2 - h_1 m$ describes the coupling to a surface field h_1 and enhancement g . In this case, the divergence theorem generalizes equation (14) to

$$H^{(0)}[m_\Xi^{(0)}] = -\frac{1}{2} \int_\psi d\mathbf{s}_\psi (m_\Xi^{(0)} - m_0) \phi_1'(m_\Xi^{(0)}) - \frac{m_0}{2} \int_{\ell^-} d\mathbf{s}_\ell \nabla m_\Xi^{(0)} \cdot \mathbf{n}_\ell - \frac{m_0}{2} \int_{\ell^+} d\mathbf{s}_\ell \nabla m_\Xi^{(0)} \cdot \mathbf{n}_\ell \quad (113)$$

where we have used the appropriate boundary condition in the integral over the wall. Similarly, the diagrammatic expansion for the constrained magnetization reads, in the DP approximation,

$$\delta m_\Xi^{(0)} = -m_0 \left(\text{diagram 1} - \text{diagram 2} + \text{diagram 3} - \dots \right) + \left(\text{diagram 4} - \text{diagram 5} + \text{diagram 6} - \dots \right) \quad (114)$$

where the black squares on the wall denote a convolution of the Green's function K with an auxiliary function $\mu(\mathbf{r}_\psi)$. This accounts for the variation of the surface magnetization, and is introduced to satisfy the boundary condition at the wall. For example, for a planar wall, μ satisfies the integral equation

$$\kappa \mu(\mathbf{r}_\psi) + 2\kappa m_0 \text{diagram 7} = g m_0 + h_1 + g \int d\mathbf{r}'_\psi \mu(\mathbf{r}'_\psi) K(\mathbf{r}'_\psi, \mathbf{r}_\psi) \quad (115)$$

which can be solved via a Fourier transform. From here, the calculation proceeds as described in [1], within the DP approximation, and similar to that described herein using perturbation

theory. The final result for the two dominant diagrams in W remains unchanged from equation (1) but with coefficients

$$a_1 = \frac{\kappa}{\kappa - g} \frac{8(h_1 m_0 + g m_0^2)}{2 - \epsilon + \sqrt{4 - 3\epsilon}} \quad b_1 = -\frac{\kappa + g}{\kappa - g} \frac{16 \kappa m_0^2}{(2 - \epsilon + \sqrt{4 - 3\epsilon})^2} \quad (116)$$

where we have expressed the results as appropriate for the potential (34). As anticipated, the diagrammatic form is very similar to that described for fixed boundary conditions but with the advantage that one can now discuss first-order wetting ($g > -\kappa$) and tricritical wetting ($g = -\kappa$). The problem of tricritical wetting is particularly interesting because the coefficient b_1 of the second diagram, Ω_1^2 , in (1) vanishes. The repulsion from the wall is then determined by a diagram which generates a term of order $e^{-3\kappa\ell}$ in the usual binding potential function. This corresponds to the next diagram in the series (90) and involves three tubes, as is discussed next.

9.4. The dominant three-tube diagram

There are several diagrams involving three tubes which contribute towards the coefficient of $e^{-3\kappa\ell}$ in $W_\pi(\ell)$. However, there is only one such diagram whose coefficient does not vanish at $t = 0$ and is, therefore, necessary for the discussion of tricriticality. The diagram in question is

$$\mathbb{V} = \kappa \int_{V_w} d\mathbf{r} \left\{ \int ds_\ell K(\mathbf{r}_\ell, \mathbf{r}) \right\}^3 \quad (117)$$

and is generated by the cubic interaction in $\Delta\phi(m)$. Here, V_w denotes the volume of the wall. This diagram is the next term in the asymptotic expansion (90) and is strongly non-local. However, analogous to our previous discussion of Ω_1^2 , the diagram simplifies and generates an effective many-body interfacial interaction between points at the interface. For example, for a planar wall, the integral reduces to

$$\mathbb{V} = \int \int \int ds_1 ds_2 ds_3 e^{-\kappa\ell(x_1)} e^{-\kappa\ell(x_2)} e^{-\kappa\ell(x_3)} T(x_{12}, x_{23}, x_{13}) \quad (118)$$

where the three-body interaction

$$T(x_{12}, x_{23}, x_{13}) \propto \lambda_{123} \exp(-\lambda_{123}(x_{12}^2 \ell_3 + x_{23}^2 \ell_1 + x_{13}^2 \ell_2)). \quad (119)$$

Here,

$$\lambda_{123} = \frac{\kappa}{2(\ell_1 \ell_2 + \ell_2 \ell_3 + \ell_1 \ell_3)} \quad (120)$$

and we have abbreviated $\ell_1 = \ell(\mathbf{x}_1)$ etc.

The fluctuation theory of three-dimensional short-ranged tricritical wetting requires a renormalization-group treatment of the flow of this three-body interaction similar to that described in [7] for the two-body term S , equation (106), pertinent to critical wetting. We note that the range of this three-body interaction also increases as the interface depins, implying that non-local effects are important at this transition.

9.5. Resummation of diagrams within DP

For wetting at a planar wall, it is in fact possible to resum all the diagrams appearing within the DP approximation, equation (22). This, again, makes use of the idea of effective many-body interactions, and is possible because in a general diagram Ω_μ^y one can integrate exactly over

any final black dot of the zigzag that is on the wall. Thus, the DP non-local Hamiltonian for wetting at a planar wall, with fixed boundary conditions, is given by

$$\frac{H_{\text{DP}}[\ell]}{\Sigma_{\alpha\beta}} = \int \text{d}\mathbf{s}_\ell (1 + t e^{-\kappa\ell})^2 + \int \int \text{d}\mathbf{s}_1 \text{d}\mathbf{s}_2 \rho(\mathbf{x}_1) M(\mathbf{x}_1, \mathbf{x}_2) \rho(\mathbf{x}_2) \quad (121)$$

where

$$\rho(\mathbf{x}) = e^{-\kappa\ell(\mathbf{x})} + t e^{-2\kappa\ell(\mathbf{x})} \quad (122)$$

and

$$M(\mathbf{x}_1, \mathbf{x}_2) = S(\mathbf{x}_1, \mathbf{x}_2; \bar{\ell}_{12}) + \int \text{d}\mathbf{s}_3 M(\mathbf{x}_1, \mathbf{x}_3) S(\mathbf{x}_3, \mathbf{x}_2; \bar{\ell}_{32}) e^{-2\kappa\ell(\mathbf{x}_3)} \quad (123)$$

and S is defined in (106). The first integral generates three local contributions: the surface area, Ω_1^1 and Ω_2^1 . At leading order, the total two-body interaction M is given by S , in which case the t independent terms in the second integral reduce to Ω_1^2 . In fact, the two-body term M is very well approximated by

$$M(\mathbf{x}_1, \mathbf{x}_2) \approx \frac{S(\mathbf{x}_1, \mathbf{x}_2; \bar{\ell}_{12})}{1 - e^{-2\kappa\bar{\ell}_{12}}} \quad (124)$$

which shows how the higher-order diagrams resum to give a hard-wall repulsion in the two-body interaction.

9.6. Full diagrammatic structure beyond DP

We have not attempted to classify diagrams that contain three or more tubes. This is much more cumbersome to do beyond the DP approximation and, with the exception of tricritical wetting studies, is largely of academic interest only. Nevertheless, such structure must exist as can be seen from the following argument. We have shown that the \mathcal{X} diagram generates a term $\kappa\ell e^{-2\kappa\ell}$ in the planar binding potential $W_\pi(\ell)$ whose coefficient is $\propto t^2$. Naively, this suggests that the mean-field excess free energy, obtained by minimizing $W_\pi(\ell)$, contains a higher-order logarithmic singularity $t^4 \ln|t|$. However, such a contribution does not exist as can be seen from the full mean-field calculation for the LGW model. This must mean that, when evaluated at the equilibrium mean-field wetting layer thickness, the term $t^2\mathcal{X}$ in W_π exactly cancels with higher-order diagrams which generate terms of order $t\kappa\ell e^{-3\kappa\ell}$ and $t\kappa\ell e^{-4\kappa\ell}$. Indeed, such diagrams can be readily identified in the perturbation theory. This is strongly suggestive that at least some higher-order diagrams can be grouped together systematically.

Further extensions and applications of this work, including a discussion of correlation function structure and the presence of long-ranged forces, will be discussed in future papers.

Acknowledgments

AOP is very grateful to Dr A Lazarides and Professor P M Goldbart for very stimulating conversations. CR acknowledges support from grants MOSAICO (Ministerio de Educación y Ciencia) and MOSSNOHO (Comunidad de Madrid). NRB acknowledges support from the Portuguese Foundation for Science and Technology (SFRH/BD/16424/2004). JMR-E acknowledges support from the European Commission (MEIF-CT-2003-501042).

References

- [1] Parry A O, Rascón C, Bernardino N and Romero-Enrique J M 2006 *J. Phys.: Condens. Matter* **18** 6433
- [2] For reviews of wetting, see Dietrich S 1988 *Phase Transitions and Critical Phenomena* vol 12, ed C Domb and J L Lebowitz (New York: Academic)
- Schick M 1990 *Liquids at Interfaces* ed J Charvolin, J F Joanny and J Zinn-Justin (Amsterdam: Elsevier) p 3364

- [3] Balian R and Bloch C 1970 *Ann. Phys.* **60** 401
Adagideli I, Sheehy D E and Goldbart P M 2002 *Int. J. Mod. Phys.* **16** 1381
Kac M 1966 *Am. Math. Monthly* **73** 1
- [4] Fisher M E and Jin A J 1991 *Phys. Rev. B* **44** 1430
Jin A J and Fisher M E 1993 *Phys. Rev. B* **47** 7365
- [5] Fisher M E and Jin A J 1992 *Phys. Rev. Lett.* **69** 792
Jin A J and Fisher M E 1993 *Phys. Rev. B* **48** 1897
- [6] Fisher M E, Jin A J and Parry A O 1994 *Bunsenges. Phys. Chem.* **98** 357
- [7] Parry A O, Romero-Enrique J M and Lazarides A 2004 *Phys. Rev. Lett.* **93** 086104
- [8] Henderson J R 2006 *J. Phys.: Condens. Matter* **18** V11
- [9] Brézin E, Halperin B I and Leibler S 1983 *Phys. Rev. Lett.* **50** 1387
Fisher D S and Huse D A 1985 *Phys. Rev. B* **32** 247
- [10] Binder K, Landau D P and Kroll D M 1986 *Phys. Rev. Lett.* **56** 2272
Binder K, Landau D P and Wansleben S 1989 *Phys. Rev. B* **40** 6979
Parry A O, Evans R and Binder K 1991 *Phys. Rev. B* **43** 11535
- [11] Greenall M G, Parry A O and Romero-Enrique J M 2004 *J. Phys.: Condens. Matter* **16** 2515
Parry A O, Rascón C and Morgan L 2005 *J. Chem. Phys.* **123** 234105
- [12] Rejmer K, Dietrich S and Napiorkowski M 1999 *Phys. Rev. E* **60** 4027
- [13] Parry A O, Rascón C and Morgan L 2006 *J. Chem. Phys.* **124** 151101
- [14] Henderson J R 1992 *Fundamentals of Inhomogeneous Fluids* ed D Henderson (New York: Dekker) chapter 2
- [15] Parry A O and Evans R 1988 *Mol. Phys.* **65** 455
Parry A O and Evans R 1993 *Molecular Phys.* **78** 1527
Boulter C and Parry A O 1995 *Phys. Rev. Lett.* **74** 3403
Parry A O and Boulter C J 1995 *Physica A* **218** 77
- [16] Abraham D B 1983 *Phys. Rev. Lett.* **50** 291
Fisher M E 1984 *J. Stat. Phys.* **34** 667
Abraham D B *et al* 1992 *Phys. Rev. Lett.* **68** 423
Abraham D B, Chayes J T and Chayes L 1984 *Commun. Math. Phys.* **96** 439
- [17] Nakanishi H and Fisher M E 1982 *Phys. Rev. Lett.* **49** 1565
- [18] Holyst R and Poniewierski A 1987 *Phys. Rev. B* **36** 5628
Gelfand M P and Lipowsky R 1987 *Phys. Rev. B* **36** 8725
- [19] Rowlinson J S and Widom B 1982 *Molecular Theory of Capillarity* (Oxford: Oxford University Press)
- [20] Helfrich W 1973 *Z. Naturf. C* **28** 693
Robledo A and Varea C 1995 *Physica A* **220** 33
- [21] Blokhuis E M and Bedeaux D 1993 *Mol. Phys.* **80** 705
- [22] König P M, Roth R and Mecke K R 2004 *Phys. Rev. Lett.* **93** 160601